THE GEOLOGICAL SOCIETY OF AMERICA®

Topographic evolution of the Eastern Alps: The influence of strike-slip faulting activity

Thorsten Bartosch[1], Kurt Stüwe[1], and Jörg Robl[2]
[1]INSTITUTE OF EARTH SCIENCES, UNIVERSITY OF GRAZ, 8010 GRAZ, HEINRICHSTRASSE 26, AUSTRIA
[2]INSTITUTE OF GEOGRAPHY AND GEOLOGY, UNIVERSITY OF SALZBURG, 5020 SALZBURG, HELLBRUNNERSTRASSE 34, AUSTRIA

ABSTRACT

We present the results of a numerical model that was used to investigate aspects of the landscape evolution of the Eastern European Alps in the Miocene. The model allows the consideration of strike-slip faulting, an inherent feature of the Miocene tectonics in the Eastern Alps, within a viscous medium. Mechanical deformation of this medium is coupled with a landscape evolution model to describe surface processes. For the input variables, the activity history of strike-slip faulting in the Eastern Alps was compiled from literature sources. The results present a major improvement in the predicted topographic development over earlier models in terms of the location and build-up of valleys and mountain ranges that form in response to the strike-slip faulting activity. Intramontane basin formation is predicted and the metamorphic dome of the Tauern Window evolves dynamically in the simulations, related to well-known east-west–striking strike-slip faults in the region. It is interesting that the metamorphic dome formation is predicted by the model without explicit consideration of the low-angle detachments bounding the dome in the west and east, suggesting that metamorphic domes can form in transpressional or strike-slip environments. The model underpredicts the mean elevation of the Eastern Alps by several hundreds of meters, which is interpreted in terms of an independent non-convergence-related event of the past 5 m.y. that has been inferred previously from other field data. Time-series analysis of elevations reveals a clear correlation between maximum height and the amount of strike-slip activity and a nonequilibrium state between uplift and erosion. We interpret this in terms of future topographical growth of the Eastern Alps.

LITHOSPHERE GSA Data Repository Item 2017083 doi:10.1130/L594.1

INTRODUCTION

The development of the Alpine orogeny is an ongoing multistage tectonic process between the stable European plate and the northeastward moving and rotating Adriatic plate (Froitzheim et al., 2008; Handy et al., 2010). The topographic evolution of this orogeny started after the final subduction of the Penninic Ocean in the Eocene and is ongoing (Hergarten et al., 2010). In the Miocene, the eastern part of this orogeny was associated with large horizontal kinematics normal to the convergence direction, mostly accommodated by orogen-scale strike-slip faults. This so called lateral extrusion of the Eastern Alps (Ratschbacher et al., 1991a, 1991b) was predominantly facilitated by the rollback of a subduction zone east of the Alps, which also opened the Pannonian Basin (Horvath and Cloetingh, 1996; Royden et al., 1983). The Miocene lateral extrusion of the Eastern Alps involved both compressional lateral escape tectonics and gravitational collapse of unstable crustal blocks (Ratschbacher et al., 1991a, 1991b), and is thought to have been intimately related to the early topographic evolution of the Eastern Alps (Frisch et al., 1998; Frost et al., 2009; Linzer et al., 2002; Robl et al., 2008b; Sachsenhofer et al., 2003; Wölfler et al., 2011). However, details of the topographic evolution since the Miocene and the interaction of topography development with the strike-slip faulting are not very well known.

In this paper we expand on an early simplified modeling study (Robl et al., 2008b) by using a refined numerical modeling approach to predict aspects of the geomorphic evolution of the Eastern Alps since the late Oligocene. In particular we consider the influence of temporal variations of strike-slip faulting activity on the development of topography. In order to obtain the input variables for the model, a time history of relevant Miocene strike-slip activity is compiled from literature sources and a geometrical reconstruction of fault geometry prior to the onset of the lateral extrusion is computed by plan-view geometrical back rectification. This information is then migrated into a finite element model and validated with current fault locations. The results of this model are interpreted in terms of their predictions for the evolution of topography in the Eastern Alps.

GEOLOGICAL SETTING

According to Nocquet and Calais (2003), the tectonic processes in the Alps during the past 30 m.y. have been dominated by a stable European plate, while the Adriatic plate is moving ~5 mm/yr in a north to northwest direction, performing a counterclockwise rotation-like movement. However, the kinematic condition for the Adriatic plate motion is not uniformly described in the literature. Decker et al. (1994) and Ratschbacher et al. (1991b) assumed a linear northward movement of a rectangular indenter, while palinspastic reconstructions (Frisch et al., 2000, 1998) imply more complex kinematics, including translation and clockwise rotation to the east of Bolzano (Fig. 1). Linzer et al. (2002)

Thorsten Bartosch http://orcid.org/0000-0003-1432-7330
*Bartosch: thorsten.bartosch@edu.uni-graz.at; Stüwe: kurt.stuewe@uni-graz.at; Robl: joerg.robl@sbg.ac.at

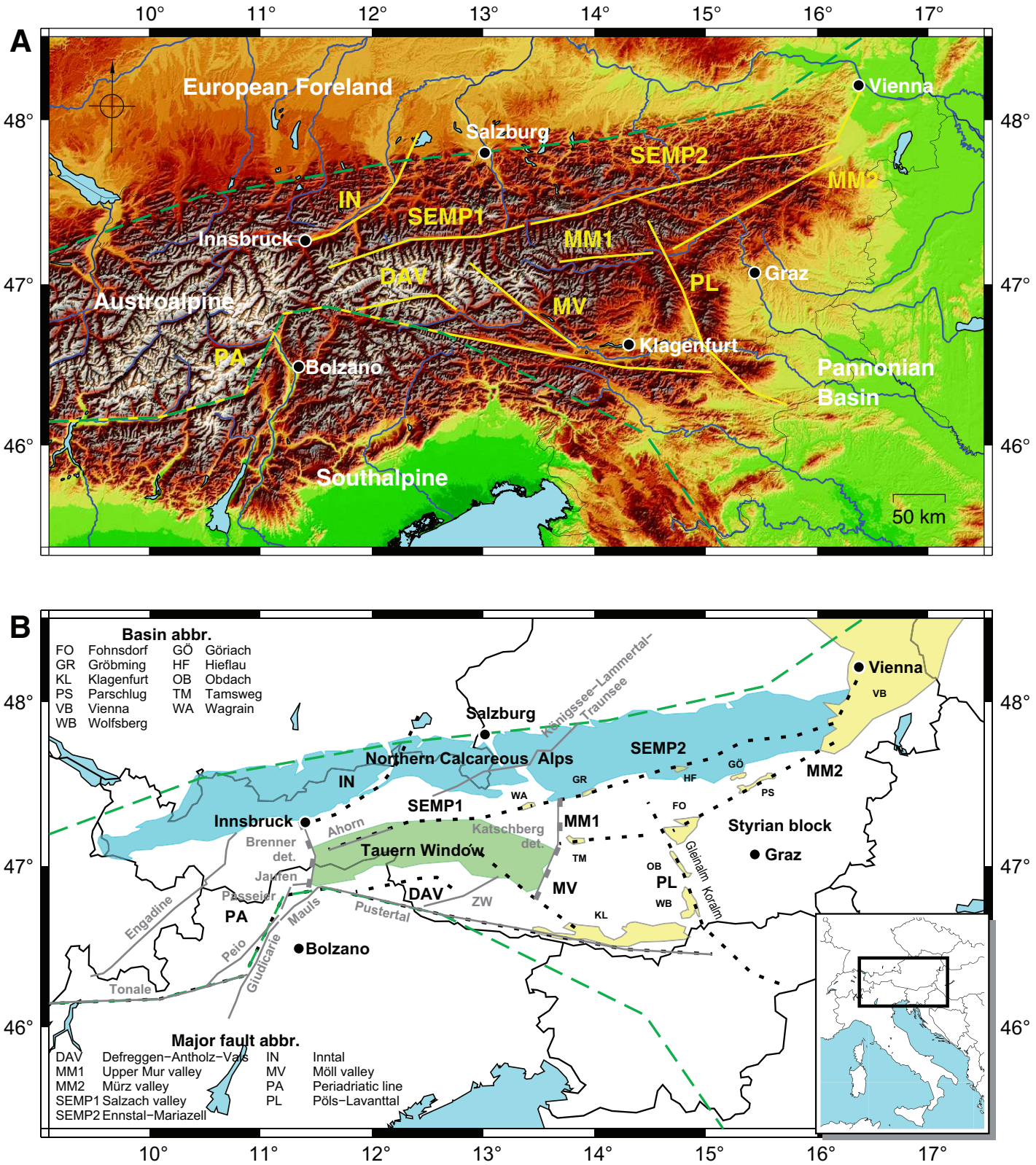

Figure 1. The simulation area of the Eastern Alps. The southwest vertex of both maps constitutes the Euler pole of the Adriatic plate. (A) Topographic map of the Eastern Alps showing the seven major fault zones considered in this study (yellow lines) and the assumed boundaries of rheology contrast (green lines). (B) Map of the same region showing the location of the Tauern Window (TW), the Northern Calcareous Alps (NCA), the most important intramontane basins, and most regional names used in the text.

estimated a linear north-northeast translational displacement of the Adriatic plate with almost no rotation. For the present-day, Nocquet and Calais (2003) estimated an exclusively counterclockwise rotation of the Adriatic plate at a rate of $\dot{\varphi} = 0.52°$/m.y. with the Euler pole being located close to Milan, Italy.

The geomorphological evolution of the Alps that accompanies this kinematic frame is the subject of much debate, but the generally accepted onset of topography development is the beginning of subsidence in the Alpine foreland basins (Linzer et al., 2002). This started ~30 m.y. ago and was largely synchronous with the final subduction of the Penninic Ocean, the head-on collision of the Adriatic and European continental plates, and the formation of a new plate boundary between the two, the Periadriatic line (Fig. 1).

Frisch et al. (1998) argued that topography development in the Eastern Alps began from a flat lowland topography in the Oligocene. Late Oligocene alluvial fans, which were fed from the Northern Calcareous Alps (NCA), can only be found to the west of the Inntal-Brenner line. The NCA east of the IN were not uplifted at that time. This is documented by remnants of conglomerates and sands (Augenstein Formation) deposited by braided river systems, today located at planation surfaces as high as 2000 m. The source of these deposits is interpreted to be a hilly (moderate elevation) low metamorphic area to the south of the eastern NCA.

Following the onset of topographic uplift, there is limited evidence about the details of the geomorphic evolution of the Eastern Alps between 30 m.y. and today. Nevertheless, it is known that intramontane basins formed during the main phase of lateral extrusion between 18 and 15 m.y. (Dunkl et al., 2005; Sachsenhofer et al., 2003). These basins formed along major strike-slip faults at the time of subsidence in the Pannonian Basin and contain terrestrial sediments. Legrain et al. (2014) documented that U-He ages from the Koralpe range are ca. 16 m.y., indicating that the tilting and early uplift of this range occurred in connection with this activity. Simultaneously, the tectonic Tauern Window (TW) was exhumed between the low-angle Brenner and Katschberg detachments and the high peaks of the Tauern range were uplifted (Fügenschuh et al., 1997; Wölfler et al., 2011, 2012). In the Samartian (12.7–11.6 m.y.) the Tauern Window was opened and from 10 m.y. onward NCA debris becomes important in Molasse sedimentation in the Eastern Alps, indicating substantial surface uplift (Frisch et al., 1998). Overall, the low-temperature geochronological data of Wölfler et al. (2012) are consistent with a more or less linear history of final exhumation and topography development for much of the region east of the Tauern Window between 17 and 5 m.y. Their data are consistent with increased sedimentation in the Molasse basins starting ca. 18 m.y., as documented by Kuhlemann et al. (2002).

Evidence has emerged that a renewed surface uplift event, uplifting the Eastern Alps by at least 500 m, commenced ca. 7–4 m.y. (Legrain et al., 2014; Wagner et al., 2010, 2011). This event is now well documented at the eastern edge of the Alps where glacial carving during the past 2 m.y. was absent, but it appears to have also affected both the northern and southern Molasse (Genser et al., 2007) and may therefore be much wider spread than is currently documented. The event appears to be of large wavelength and unrelated to fault activity. While it has been argued that the young uplift of the Alps may correlate with erosional unloading due to glacial erosion (Champagnac et al., 2007), the event commenced earlier than the glaciation periods. However, the event correlates with a dramatic spike in the sedimentation rates in the basins surrounding the Alps that started ca. 5–4 m.y. (Kuhlemann, 2007; Kuhlemann et al., 2001, 2002).

ACTIVITY OF STRIKE-SLIP FAULTING IN THE EASTERN ALPS

In the Eastern Alps, strike-slip faulting is intimately related to the development of topography (Frisch et al., 1998; Frost et al., 2009; Linzer et al., 2002; Ratschbacher et al., 1991a, 1991b; Robl et al., 2008b; Sachsenhofer et al., 2003; Wölfler et al., 2011). We therefore provide a summary of the Miocene strike-slip activity here. For simplicity we consider only seven major faults, the Periadriatic (PA), Defreggen-Antholz-Vals (DAV), Möll valley (MV), Salzach-Ennstal-Mariazell-Puchberg (SEMP), Inntal (IN), Mur-Mürz valley (MM), and Pöls-Lavanttal (PL) (Fig. 1). All relevant activity ages are collated in Table 1. Other than these mostly Miocene strike-slip faults, there are two north-south–striking shallow-angle detachments that are largely synchronous and bound the Tauern Window to the west and east: the Brenner line and the Katschberg line (Fügenschuh et al., 1997; Genser and Neubauer, 1989). Both also play a role in the topographic evolution of the Eastern Alps, but we show here that they formed dynamically in response to the strike-slip zone activity and need not be explicitly considered.

The PA bounds the Eastern Alps to the south and is the most important large-scale fault system of the Alps (Fig. 1). It is interesting that the southern boundary of alpine metamorphism does not follow the PA, but is located north of it within the Austroalpine, partly along the DAV fault (Müller et al., 2001). However, the PA separates the rheologically somewhat softer Eastern Alps from the somewhat stronger Southalpine unit over a length of ~700 km (Robl and Stüwe, 2005b). In the target region, it consists of several faults (locally named the Tonale, Giudicarie, Mauls, and Pustertal). Based on fault gouge and pseudotachylite dating, Müller et al. (2001) revealed variable activity for individual parts of the fault. Two time frames, from 32 to 29 m.y. for the North Giudicarie (thrusting), Tonale, and Pustertal, and 22 to 16 m.y. for the Tonale, Pustertal, Jaufen, and Passeier faults are most striking (Table 1). Zwingmann and Mancktelow (2004) dated illites in mylonites in the Mauls fault as 16 m.y. and also considered the nature of individual fault segments of the PA to be noncoeval. Additional minor times of activity that are shown in Figure 2 are listed in Table 1 for the PA and all other faults discussed in the following.

The DAV extends for ~80 km in an east-west direction to the south of the Tauern Window and north of the PA (Pustertal, Mauls faults) (Fig. 1). It constitutes the southern border of alpine metamorphism and shows dominant sinistral and subordinate normal faulting kinematics (Müller et al., 2000). Pseudotachylite dating revealed two major phases of activity at 33–29 m.y. and 26 m.y. (Müller et al., 2001) (Table 1). Wölfler et al. (2011) inferred eastward extrusion of the Austroalpine unit with major displacements along the IN, DAV, and PA from eastward-moving activity patterns and kinematic settings of the faults. In general, few time constraints are available for faulting of the DAV and all other faults between the Tauern Window and the PA.

To the south of the Tauern Window there is a network of fault zones with varying kinematic sense (Fig. 1). The dextral MV, which shows an offset of ~2.5 km, constitutes the eastern margin; it strikes along 80 km in a northwest direction and cuts into the Tauern Window at its southeastern end. According to Wölfler et al. (2011), the main vertical kinematic activity (exhumation) of this fault zone was between 27 and 25 m.y. and a second activity pulse occurred at 21 m.y. Wölfler et al. (2011) suggested that their data can be interpreted in terms of warping of isotherms and therefore with surface uplift that occurred in connection with this exhumation event. Time constraints about horizontal activity are not well known. The activity time frame was extended to 31–22 m.y. by Inger and Cliff (1994).

The SEMP has a total length of ~400 km, extends approximately in the west-east direction, and constitutes the second-largest tectonic structure in the Eastern Alps. It is thought to have accumulated ~60 km of sinistral strike-slip displacement (Urbanek et al., 2002). For much of its length, it separates the Mesozoic NCA from crystalline basement of the middle Austroalpine units to the south and formed a number of pull-apart

TABLE 1. SYNOPSIS OF TEMPORAL ACTIVITIES AND KINEMATICS OF GEOLOGICAL STRUCTURES OF THE EASTERN ALPS FROM VARIOUS LITERATURE RESOURCES

Name	Activity* (m.y.)	Type	Remark	Reference
Tauern window	24–22, comp.	uplift		Kuhlemann (2007)
	18–15, comp.	uplift		Kuhlemann (2007)
	31.2 ± 0.4	sinistral	Olperer fault	Glodny et al. (2008)
	26.7 ± 1.2, 21.5 ± 0.8	sinistral	Greiner fault	Glodny et al. (2008)
	19.8 ± 0.4	sinistral	Ahrntal fault	Glodny et al. (2008)
	31–30	slightly sinistral	ductile, eclogite zone	Glodny et al. (2008)
	5	uplift	Carpathian slab break off 10–7 m.y.	Wölfler et al. (2012)
Defreggen-Antholz-Vals	46.1 ± 3.1	sinistral	Zinsnock area	Mancktelow et al. (2001)
	33.4 ± 1.9, 30.1 ± 4.6	sinistral		Müller et al. (2000)
	32–30, 25.5 ± 0.9	sinistral		Müller et al. (2000)
Engadine	late Oligocene	sinistral	4 (southwest)–20 (northeast) km	Linzer et al. (2002)
Inntal	33–23	sinistral	34–48 km, thin skinned	Linzer et al. (2002)
Königssee-Lammertal-Traunsee		uplift, sinistral	10 km, thin skinned, uplift 0.7–2 km	Linzer et al. (2002)
Mur-Mürz valley	17–13	pull–apart	sedimentation	Dunkl et al. (2005)
	17	sinistral	change to normal faulting	Reinecker (2000)
	17–14	sinistral	major subsidence	Ratschbacher et al. (1991b)
Möll valley	31–22	no uplift	localized deformation	Inger and Cliff (1994)
	25.3 ± 2.9, 20.7 ± 2.3	Dextral		Glodny et al. (2008)
	27–25, 21	uplift, dextral	2.5 km	Wölfler et al. (2011)
Periadriatic line	32–29, 18–13	dextral	60 km	Wölfler et al. (2011)
	29.88 ± 0.29	sinistral	Jaufen Passeier	Müller et al. (2000)
	32, 21, 16	dextral	Tonale	Müller et al. (2001)
	32–29	thrusting	Northern Giudicarie fault	Müller et al. (2001)
	17	sinistral	Passeier	Müller et al. (2001)
	32–30, 21–17	sinistral	Jaufen	Müller et al. (2001)
	27	dextral	Mauls	Müller et al. (2001)
	22–20	dextral	Pustertal	Müller et al. (2001)
	20.1 ± 2.2	sinistral	Speikeboden (Periadriatic splay fault)	Mancktelow et al. (2001)
	23.5–19	dextral	Tonale fault	Zwingmann and Mancktelow (2004)
	16	dextral	Mauls fault	Zwingmann and Mancktelow (2004)
	9–6	dextral	(Tonale), Centovally, Simplon	Zwingmann and Mancktelow (2004)
	17	sinistral	Northern Giudicarie fault	Pleuger et al. (2012)
Pöls-Lavanttal	18–16, 14–12	dextral	8–10 km	Reinecker (2000)
	11–5.5	dextral	8–10 km	Reischenbacher and Sachsenhofer (2013)
Ahorn shear zone	12–7	sinistral	ductile, 2 km wide, part of SEMP	Rosenberg and Schneider (2008)
	15.7 ± 1.3	sinistral	ductile, part of SEMP	Glodny et al. (2008)
	19.15 ± 0.03, 17.04 ± 0.3	sinistral	Stillup valley	Schneider et al. (2007)
Salzach	35–28	sinistral	60 km, Salzach (35–28 m.y.), Hieflau (17 m.y.)	Urbanek et al. (2002)
Ennstal-Mariazell-Puchberg	23–12	sinistral	lateral extrusion main phase	Ratschbacher et al. (1991b)
	17–14	sinistral		Dunkl et al. (2005)
	18–15	sinistral	intramontane basins	Linzer et al. (2002)
	118–9 ka	sinistral	flowstone deformation	Plan et al. (2010)
Zwischenberg-Wöllatratten	Oligocene	sinistral		Wölfler et al. (2012)

*Ages in m.y., except for last (118–9 ka)
Note: comp.—compression; SEMP—Salzach-Ennstal-Mariazell-Puchberg fault.

basins (e.g., Wagrain, Gröbming, Hieflau) during Oligocene to Miocene activity. Many sinistral strike-slip faults branch from the SEMP toward the northeast (Decker et al., 1994; Ratschbacher et al., 1991b). The Salzach valley part of the fault cuts into the northwestern part of the Tauern Window and changes into the ductile, as much as 2 km wide, Ahorn shear zone, which dies out ~15 km east of the Brenner normal fault (Frost et al., 2009; Rosenberg and Schneider, 2008). Urbanek et al. (2002) published mylonitic marble ages for the SEMP line that indicate activity between 35 and 28 m.y. According to Ratschbacher et al. (1991b) the main activity time frame of the SEMP, which correlates with the main lateral extrusion phase, is late Oligocene to middle Miocene (23–12 m.y.). However, Dunkl et al. (2005) and Decker et al. (1994) documented intramontane basin sedimentation ages between 18 and 14 m.y. that were used in this study.

The sinistral IN commences as the Engadine fault in the west and accumulated ~31–50 km of strike-slip displacement between 32 and 23 m.y. within a thin-skinned tectonic setting (Linzer et al., 2002). The fault dies out in the Molasse foreland basin to the east. The IN is one of several strike-slip faults (e.g., the Königssee-Lammertal-Traunsee fault) cutting the NCA in northeast directions related to lateral extrusion and north-south shortening of the NCA during the second alpine orogeny (Frisch et al., 1998).

The sinistral MM is also known as the Noric Depression. The fault extends for ~250 km from the eastern end of the Tauern Window to the south of the Vienna Basin (Fig. 1). Together with the PL it forms a conjugate strike-slip fault set

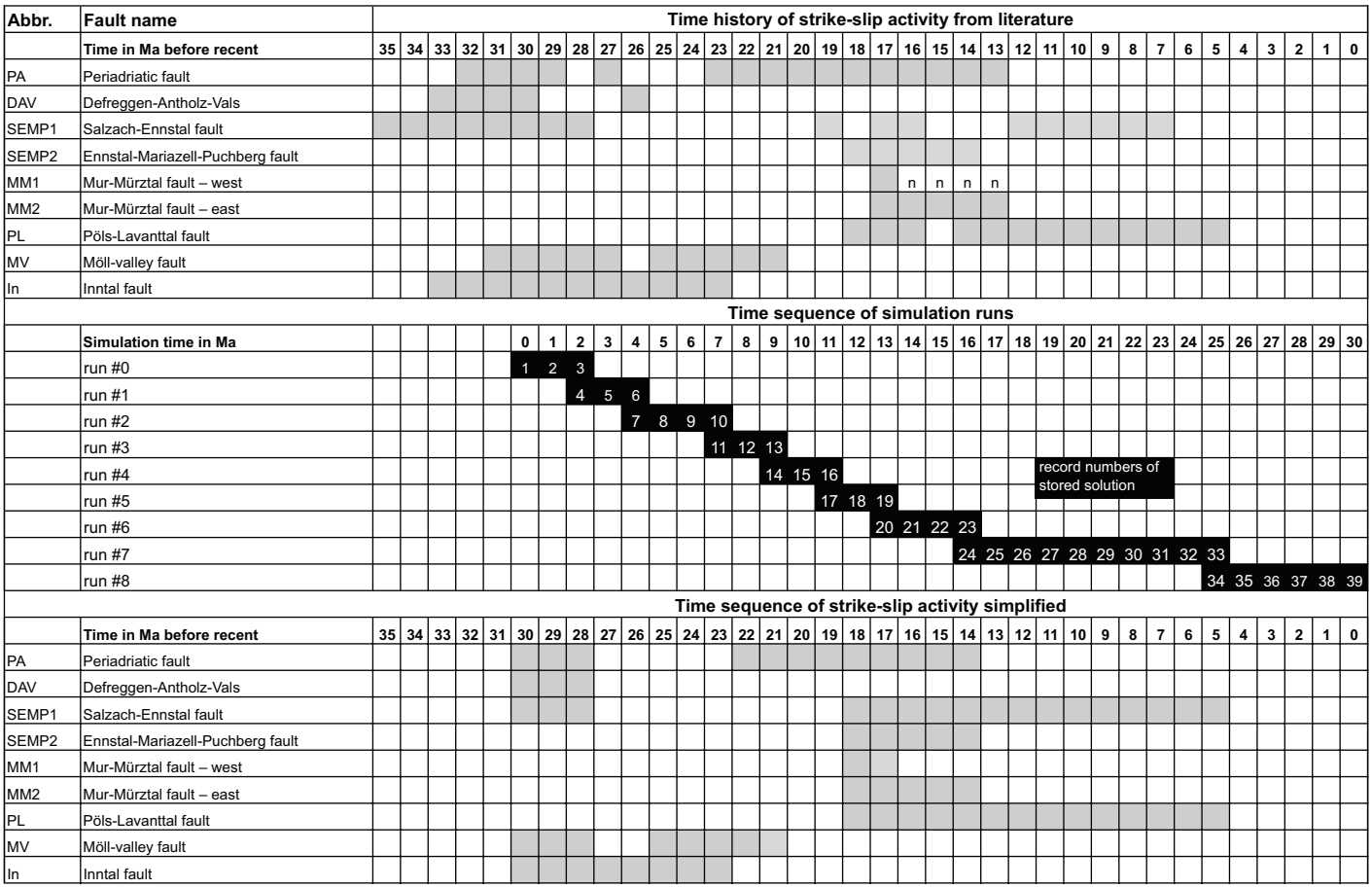

Figure 2. Summary of the major Miocene strike-slip faulting activity in the Eastern Alps (Abbr.—abbreviation). The top panel shows the activity from the literature as detailed in Table 1; shaded boxes indicate active (open) and white boxes indicate inactive (closed). The symbol n indicates normal faulting. The middle panel shows how the Tertiary evolution was discretized into nine selected time slices for the simulations. During each time slice, no changes in fault activity are assumed. The bottom panel shows the simplified activity history as used for the nine time slices of the simulations.

pushing the Styrian block to the east. The MM formed at the beginning of lateral extrusion in early to middle Miocene time (Linzer et al., 2002; Sachsenhofer et al., 2003). A series of pull-apart basins formed along the Mur-Mürz valley (Reinecker, 2000; Strauss et al., 2001). Their sedimentary records allow the dating of its activity. Dunkl et al. (2005) gave an activity period of 17–13 m.y., consistent with a sedimentary date of 16 m.y. and a slip accumulation of 30 km by Linzer et al. (2002). Wölfler et al. (2011) suggested a kinematic separation of the MM into two segments west and east of the PL system. Both are supposed to have initiated with strike-slip activity before 16 m.y. Afterward only the eastern part keeps its lateral tectonics, while the western part changes into a normal fault, extending the Katschberg detachment and causing the hanging-wall Gurktal block to slip in southeast direction (Wölfler et al., 2012). Surface uplift of the entire region south of the Noric Depression and east of the PL is likely to be connected to the fault activity in the Miocene and is evidenced by paleolandscapes today above ~1100 m above sea level. This paleolandscape was uplifted to its present elevation after 5 m.y. (Wagner et al., 2010, 2011).

The PL is a dextral fault system consisting of several parts (Fig. 1). It extends north-northwest for ~150 km and separates the Saualpe from the Koralm complex. Both parts, the northern Pöls fault with a slip accumulation of ~8 km and the southern Lavanttal fault with a slip displacement of 10 km, are dying out in the Fohnsdorf Basin and cross the MM in this zone (Frisch et al., 2000). From the sediment record in small associated pull-apart basins (Wolfsberg and Obdach), its activity was Karpathian to mid-Pannonian (Reischenbacher et al., 2007; Reischenbacher and Sachsenhofer, 2013). Due to drill core age dating results from cataclasites and fault gouges, the age of its activity is well known, compared to the less-well-known activity of the conjugate MM. According to Kurz et al. (2011), Reinecker (2000), and Reischenbacher and Sachsenhofer (2013), the fault was active ca. 18–16 m.y., ca. 14–12 m.y., and between 11 and 5.5 m.y. Observed seismic events, which indicate recent activity of this fault, were not taken under consideration for this analysis.

THIN VISCOUS SHEET AND LANDSCAPE EVOLUTION MODELING

In order to model the influence of strike-slip faulting on topography development in the Eastern Alps, we have expanded an existing finite element code that is based on a viscous sheet formulation. The thin viscous sheet formulation was introduced by England and McKenzie (1982, 1983) and assumes a two-dimensional sheet that deforms according to a generalized power law rheology:

$$\tau_{ij} = B\dot{E}^{\frac{1}{n}-1}\dot{\varepsilon}_{ij}, \quad (1)$$

the deviatoric stress $\tau_{ij} = \sigma_{ij} - p\delta_{ij}$, the strain rate tensor is $\dot{\varepsilon}_{ij}$, the second invariant of the strain rate tensor $\dot{E} = \sqrt{\dot{\varepsilon}_{kl}\dot{\varepsilon}_{kl}}$, and B is a material constant;

σ_{ij} and $p = \sigma_{ii}/3$ are the stress tensor and the lithospheric pressure, and δ_{ij} is the Kronecker symbol. The indices i, $j = 1(1)3 \in \mathbb{Z}$ represent the Cartesian coordinates. Double indices within a term imply a summation according to the Einsteinian summation rule. The thin viscous sheet model based on this rheology has successfully been used to describe the India-Asia collision zone (England and Houseman, 1986) and the Alps (Robl and Stüwe, 2005b) and is briefly summarized here.

The static momentum equation forms the basis of the mechanical modeling and is given by:

$$\frac{\partial \tau_{ij}}{\partial x_j} + \frac{\partial p}{\partial x_i} = \rho g \delta_{i3}, \quad (2)$$

with gravity acting in $-z$ direction and p being negative for compression. Neglecting all vertical gradients of deviatoric stress and assuming isostasy, the thin viscous sheet formulation is derived by averaging across the lithosphere (England and McKenzie, 1983; Houseman and England, 1986). After normalization this results in:

$$A_r \frac{\partial s_c^2}{\partial x_i} = \frac{\partial}{\partial x_j}\left[\eta\left(\frac{\partial u_i}{\partial x_j} + \frac{\partial u_j}{\partial x_i}\right)\right] + \frac{\partial}{\partial x_i}\left[2\eta\left(\frac{\partial u_1}{\partial x_1} + \frac{\partial u_2}{\partial x_2}\right)\right] \forall i, j = 1,2\ . \quad (3)$$

In this equation $\dot{\varepsilon}_{ij} = \left(\partial u_i / \partial x_j + \partial u_j / \partial x_i\right)/2$ is the strain rate tensor, $\eta = \left(\dot{E} s_1 / u_0\right)^{\frac{1}{n}-1}$ the dimensionless viscosity and $A_r = \frac{g\rho_c\left(1-\frac{\rho_c}{\rho_m}\right)s_1}{B\left(u_0/s_1\right)^{1/n}}$.

The Argand (A_r) number with the normalization constants u_0 and s_1 (velocity and initial lithosphere thickness) summarizes all material constants and can be interpreted as a ratio of vertical and horizontal stresses. For $A_r > 1$ the orogeny is dominated by gravitational collapse, whereas for $A_r < 1$ a kinematic control by boundary condition is given. The thin viscous sheet assumption reduces the indices to $i, j = 1(1)2 \in \mathbb{Z}$ representing the x_1 and x_2 plan-view coordinates only. Equation 3 constitutes a two-dimensional partial differential equation for the velocity field, which can be solved by Galerkin finite element approximation. For all $n \neq 1$ this nonlinear scheme is solved iteratively with recalculated η after each step. Although Equation 3 is strictly two-dimensional in plan view, a crustal thickness distribution $s_c(x, y)$ can be calculated for each time step from the continuity equation (not shown here). These calculations are done using a finite element code (used initially in Houseman and England, 1986; Robl and Stüwe, 2005a, 2005b; Robl et al., 2008b; Stüwe et al., 2008).

Following Robl and Stüwe (2005b; see also Stüwe, 2007), the topographic height h (initial height h_0) is calculated from lithospheric layer thickness s_1, the initial thickness s_1^0, and initial crust thickness s_c^0 using:

$$h = \left(s_1 - s_1^0\right) s_c^0 \frac{\rho_m - \rho_c}{\rho_c} + h_0 \quad (4)$$

when isostatic compensation is assumed. In Stüwe et al. (2008) this model was expanded by coupling a landscape evolution model with the thin sheet model; for their erosion model they followed the common assumption that the erosion rate $\dot{h}_e$ of a given spatial location is proportional to the upstream drainage area A and the square of slope dh/dL; L is the distance along a river channel, as implemented in many landscape evolution models (e.g., Hergarten et al., 2010; Robl et al., 2008a; Stüwe, 2007; Stüwe et al., 2008; Wobus et al., 2006). This assumption may be written as:

$$\dot{h}_e = \frac{dh_e}{dt} = -eA\left(\frac{dh}{dL}\right)^2. \quad (5)$$

In this equation e is a constant erosion parameter, chosen to be $e = 2500\ m^{-1}s^{-1}$.

In order to describe brittle faulting within the viscous medium, we assume the strike-slip faulting model of Barr and Houseman (1996), which allows free slip along a fault line with a vertical fault plane and only transfers normal stresses across the fault. In the finite element code, the faults are implemented as two parallel mesh lines. The nodes on both sides move independently according to the different stress fields. Therefore, the local amount of slip along a fault line depends on the actual stress field caused by the deformation process. In other words, slip and topography along the faults form implicitly by the model. As the model is two-dimensional, the fault model is considered to be valid only for deep-rooted faults, which also cut through the most competent upper mantle lithosphere. In order to account for temporally varying fault activity after the deformation is already in progress, we divide the simulation time into time segments, during which a certain set of faults is active (Fig. 2). Additional code adaptions were required in order to handle large deformation along faults and to enable the control and/or change of the fault state when a subsequent simulation run is started based on a previous deformation. The actual implementation does not allow the handling of fault propagation. However, in view of the geologically limited resolution of fault activity, there is no need to consider their growth. Nevertheless, we segmented some fault lines into parts that are turned on and off during successive time increments according to geological knowledge. This applies in particular to the SEMP and MM faults. Between adjacent fault tips a small gap (1–5 km) is placed, because of the finite element program requirements. This limitation introduces some additional resistance against free strike slip and therefore inhibits the lateral extrusion in general. For the conjugate MM and PL fault set around the Fohnsdorf Basin in particular, we decided to inhibit the MM fault because for the past 16 m.y. its activity is known to be different between both sides of the PL.

Initial and Boundary Conditions

For the modeling, a region between long 9.1° and 17.5° and lat 45.36° and lat 48.5° is chosen (Fig. 1) and assumed to be in plane geometry. The lower left corner of this region is near the Euler pole of the Adriatic plate at 45.36°N, 9.10°E (Nocquet and Calais, 2003) and is here assumed to correspond to the Cartesian coordinate system origin. The region largely corresponds to that chosen in Robl and Stüwe (2005b) so that the results can be directly compared. Also following these earlier studies, we consider three rheological distinct regions with different viscosities, that we name European foreland (eu), Austroalpine (aust), and indenter (adr) (green polygons in Fig. 1). The dimensionless viscosity contrast parameters are chosen to $\eta_{adr,aust,eu}/\eta_{aust} = 1.5:1:3$. The Argand number is chosen as $A_r = 1$ and $n = 1$, which results in the best fit in terms of the width of the orogenic wedge and kinematics that match today's global positioning system velocity field and principal stress orientation (Robl and Stüwe, 2005b; Robl et al., 2008b). The exponent choice $n = 1$ reduces Equation 1 to a linear Newton fluid rheology. According to Barr and Houseman (1996) this rheology correlates to that of olivine at high temperatures and low deviatoric stresses and may therefore be appropriate for the alpine lithosphere as a whole.

In Robl and Stüwe (2005b) and Robl et al. (2008b) it was shown that the Nocquet and Calais (2003) findings can be used as a constant southern boundary condition for the indenter for the past 30 m.y. if one restricts the modeling area to east of the Euler pole. In the present work the best fit is found for an indenter length of 400 km. Along this length the angular velocity $\omega = 0.52°$/m.y. is interpolated into a local velocity using

$$\vec{v}\left(x[km]\right) = \frac{x}{400}(3.6,\ -0.5)^T \text{ mm / yr}$$

by linear approximation of the motion between the initial and the finite deformation state after 30 m.y. of rotation; x is the lateral coordinate of

the model and $(3.6, -0.5)^T$ means the transposing of a vector. The indenter velocity setting only holds exactly for straight rotational axes through the Euler pole. Note that the southern boundary condition of our model is assumed to be located substantially south of the present-day plate boundary at the PA (Fig. 3). Thus, the rheology contrast at the PA (with the region south of it being substantially stronger than the Eastern Alps) imposes an effective internal boundary at the PA, so that the model is robust toward crude approximations of the southern model boundary. The western boundary is fixed to allow slip in the north-south direction, but no westward motion. The eastern boundary is set to have an open boundary condition, which reflects the free extrusion constraint in Robl et al. (2008b) (see Fig. 2B middle trace).

In order to extract a surface elevation h from Equation 4 from the thin sheet layer thickness s_c, we assume that the initial lithosphere layering is a buildup of s^0_c = 35-km-thick crust and a s^0_l = 100-km-thick lithosphere with the densities ρ_c = 2700 kg/m^3 and ρ_m = 3300 kg/m^3 for the lithospheric mantle. From A_r = 1 and with the chosen normalization u_0 = 500 km/100 m.y. = 5 mm/yr, the matrix viscosity is (η = 1) B ≈ 3 · 10^{23} Pa·s. A flat topography of 100 m above sea level (the hilly surface at 30 m.y.; Frisch et al., 1998) is assumed as initial condition for h_0 so that all modeled topography, drainages, and morphologies, except the initial fault locations, are dynamically developed during the model runs. The choice to start the simulation 30 m.y. ago is reinforced by a reversal of the PA fault kinematic from sinistral to dextral, a property that cannot be controlled by the presented simulation, within the time frame of 32–30 m.y. (Mancktelow et al., 2001).

Modeling Miocene Faulting

In order to insert the relevant fault activity into the model, we have coarsened the Miocene fault activity collated in Table 1 (top panel of Fig. 2) into a scheme of nine consecutive time slices during which there is no change in faulting activity (middle panel in Fig. 2). The run for each time slice uses the final results of the predecessor run as its initial condition and faults are activated (also called open) or deactivated (also called closed). The assumed constant strike-slip activity within each run is shown in the bottom panel of Figure 2. For this, some adaptations of the fault activity were necessary.

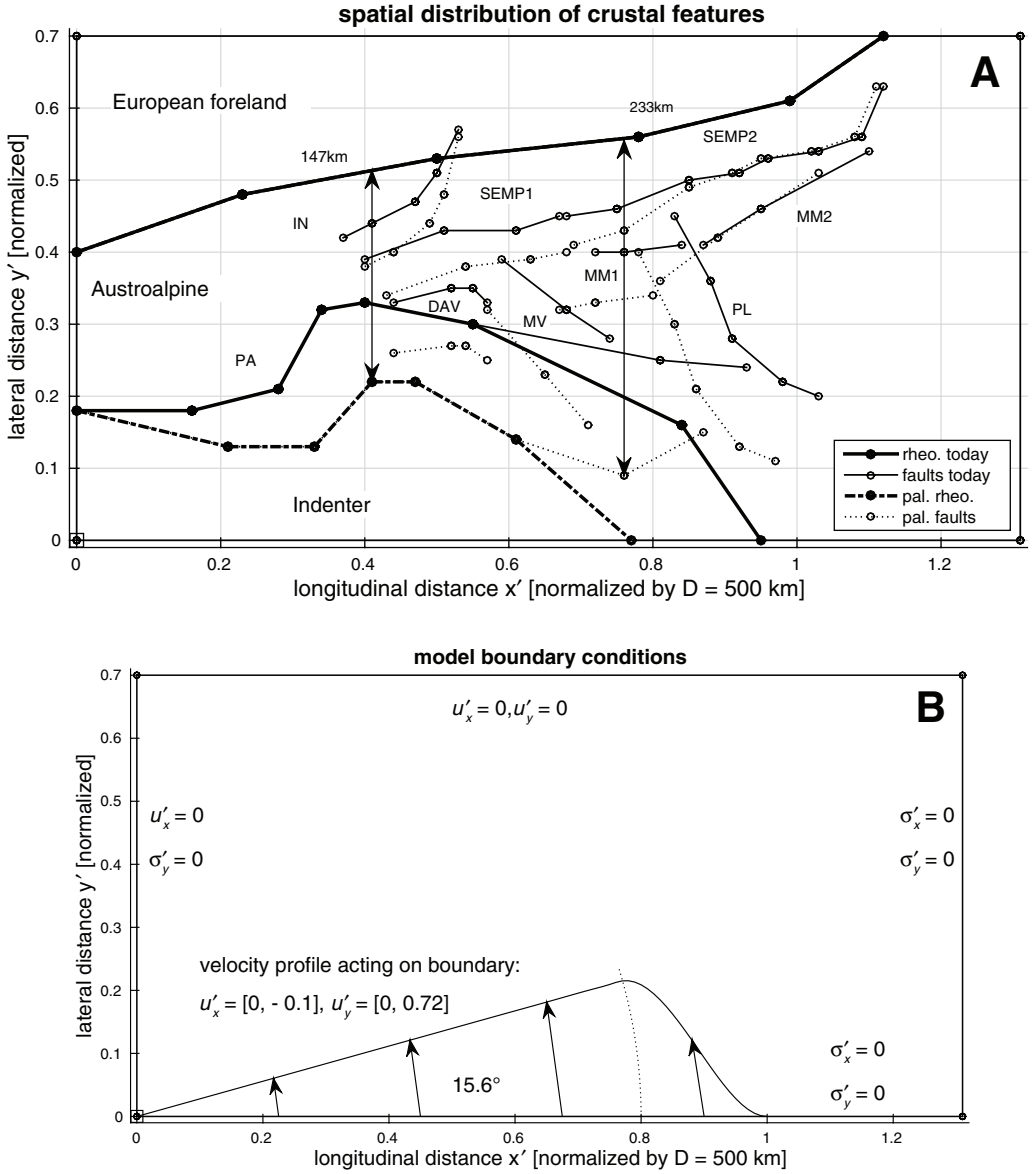

Figure 3. The model boundary conditions. See Figure 2 for fault abbreviations. (A) The spatial distribution of dominant strike-slip faults and rheology contrasts within the model boundary (outer box) based on normalized coordinates using length scale normalization D = 500 km, u_0 = 5 mm/yr (velocity). The Paleogene initial model for the simulation after rectification is shown using dotted lines for the faults and dashed lines for the viscosity contrast line. The Adriatic plate Euler pole is located at the lower left boundary vertex. The two double arrows measure the distance between the foreland and the Paleogene Periadriatic fault (PA). (B) The boundary conditions of the model (see text). The northern edge is stiff, while the southern edge approximates the rotational indenter and a free slip condition to the east of it. The western boundary allows free movement in the north-south direction. The eastern boundary is open (free of stresses).

Following Wölfler et al. (2011) it is assumed that the western part of the SEMP fault shows an early activity between 35 and 28 m.y. After a phase of inactivity the complete fault line becomes active again in 18–14 m.y. Therefore, this fault is divided into two branches (Fig. 1): the Salzach-Ennstal branch in the west (SEMP1) and the Ennstal-Mariazell-Puchberg branch in the east (SEMP2). For a similar reason the MM is segmented. According to Wölfler et al. (2011), a time frame from 18–17 m.y. is derived in which both parts of the fault are active, and between 16 and 13 m.y. only the eastern segment (MM2) is assumed to be active.

A problem with the placement of strike-slip faults in the model geometry is that their location and shape prior to Miocene shortening would need to be known. We approximate this by rectification of today's fault maps (excluding PA) and plate boundaries by back rotation around the Euler pole with the angle:

$$\phi_{\text{back}}(P_{\text{ft}}) = \begin{cases} \dfrac{\phi^{\max}}{150\ \text{km}} D(P_{\text{ft}}),\ 0 < D(P_{\text{ft}}) < 150\ \text{km} \\ 0,\ \text{otherwise} \end{cases}, \quad (6)$$

with the normal distance D in kilometers between a point P_{ft} at a recent fault and the unrotated viscosity contrast line, which largely follows the PA, and a pure translational component, which corrects for the predominantly east-west displacement due to lateral extrusion. The maximum angle $\varphi^{\max}$ is determined by experiment and is chosen as $\varphi^{\max} = -15.6°/2,\ \forall x > 0 \wedge x < 425$ km, and changing to $\varphi^{\max} = -15.6°/4,\ \forall x > 425$ km, which means an unsteady transition at the PL in an east-west direction (rotational decoupling). Figure 3A shows the actual location of the regarded fault system, while the approximated situation 30 m.y. ago is shown by dotted lines. The literature reports different palinspastic reconstruction models (Frisch et al., 2000, 1998; Linzer et al., 2002), but here we follow the Nocquet and Calais (2003) indenter back rotation assumption, which is assumed to have been constantly acting during the past 30 m.y. (Robl and Stüwe, 2005b; Robl et al., 2008b). The application of Equation 6 results in a drastic reduction of the rotational influence with increasing distance to the indenter, which dies out east of the Fohnsdorf Basin. By experiment a vector $\vec{\mathbf{T}}$ is chosen individually for each fault line in order to get the best fit between the final simulation and the today's fault geometry. All rectification parameters are given in Table 2. A steady increase of lateral extrusion from 5 km in the east to 35 km in the west at the PL is observed. The rotation angle is greatest at locations close to the PA. In Figure 3A two north-south–directed distances between the Paleogene PA and the foreland boundary are measured as 147 km at the PA knee and 233 km around the Fohnsdorf Basin. Linzer et al. (2002) gave ~156 km and 230 km for these distances, which comes close to the suggested rectification performed here.

TABLE 2. RECTIFICATION TRANSFORMATION OF STRIKE-SLIP FAULTS 30 MY

Fault name	–ϕback (°)	$\vec{\mathbf{T}}$ (km)
In	1–5.8	$(-5, 0)^{\mathsf{T}}$
SEMP1	3.4–6.4	$(-5, 0)^{\mathsf{T}}$
SEMP2	0–3.3	$(-5, 0)^{\mathsf{T}}$
DAV	6.5–7.7	$(-20, -5)^{\mathsf{T}}$
MV	5.1–7.2	$(-30, -10)^{\mathsf{T}}$
MM1	1.5–4.4	$(-35, -10)^{\mathsf{T}}$
MM2	0–1.5	$(-35, -15)^{\mathsf{T}}$
PL	2.2–3.8	$(-35, -10)^{\mathsf{T}}$
PA	15.6	$(0, 0)^{\mathsf{T}}$

Note: Angles $-\phi$ back describe a back rotation; vector **T** describes a translation. See text for fault names.

The implicit assumption of the two-dimensional model is that the modeled faults cut the entire lithosphere. It is interesting that Brückl et al. (2010) observed from mantle tomography data that structural discontinuities in the lithospheric mantle appear to mimic the location of several of the Miocene faults mapped on the surface. Therefore, we believe that our assumption is justified.

RESULTS

The simulation run shown in Figure 4 describes the model evolution of topography of the Eastern Alps for 8 different time steps, starting 30 m.y. ago and ending with a prediction of the future in +5 m.y. Figure 5 shows the vertical strain rates as a proxy for uplift rate for the same time steps. In very general terms, the Miocene strike-slip faulting activity caused uplift near transpressional ends of faults and subsidence near transtensional ends of faults, thereby facilitating drainage development in these regions and dissection of the Eastern Alps into individual blocks. At 30 m.y. the vertical strain rate in Figure 5 indicates strongest uplift north of the eastern end of the PA but little uplift for the Tauern Window region, despite the activity (open state) of the DAV and SEMP1 faults, but inactive (closed state) MV fault.

At 25 m.y. (after 5 m.y. of indentation), the highest elevations are found close to the indenter tip (west to the Klagenfurt Basin), in the Tauern Window adjacent to the MV and the DAV (close to Mount Großglockner location) and to the east of the Inn valley. The entire Eastern Alps starts to uplift sharply at both viscosity contrasts. While areas close to fault tips of the IN, MV, and DAV show increased uplift and subsidence due to strain accumulation, this can hardly be observed for the SEMP1, which is inactive at 25 m.y. A pulse of uplifting strain rate in the Tauern Window close to the later Großglockner location and Nockberge is observed due the active MV (see Fig. 5).

In the early Miocene (20 m.y.) there is a phase of relative silence in terms of strike-slip activity, and a uniform elevation increase occurs. The highest elevations, to 912 m, can be found between the southern end of the MV fault and the PA. The topographic mean height of the orogenic wedge reaches 289 m. Only the PA is active, which results in high uplift rates to the north of Bolzano and west of Klagenfurt. The MV and IN became inactive and the Tauern Window uplifted moderately, which can best be seen by small vertical strain rates. Erosion starts to form valley systems that reflect roughly the locus and geometry of the Drau, Inn, Enns, and Adige valley systems.

In the middle Miocene (15 m.y.) the activity pattern propagates further eastward. Most faults close to the Tauern Window except the SEMP1 are inactive. The vertical strain rate of this time frame shows a clear stagnation in the central Eastern Alps, consistent with extensional exhumation of the Tauern Window at this time, as documented by geochronological investigations of the bounding detachments at Brenner and Katschberg (Fügenschuh et al., 1997). Strong and spatially extended subsidence occurs around Vienna, predicting the early formation of the Vienna Basin. Localized strong subsidence can also be observed at locations that roughly correlate with intramontane basins along the PA, PL, and SEMP. In general, due to the activation of the conjugate fault set of PL and MM2, a moderate and localized uplift of the Styrian block to the west of the PL (Gleinalm, Koralm) and to the southeast of the Mürz valley is observed. Figure 4 shows a continuous rise of mean elevation to 374 m and a strong uplift, with elevations close to 800 m north to the SEMP2 near Schladming (Dachstein region). Valley incisions of the Salzach-Ennstal, the Pöls-Lavanttal, and faintly in the Mur-Mürz valley become visible.

In late Miocene time (10 m.y.) most strike-slip activity, except the PL line and SEPM1, has died out (Fig. 2). In general, uplift rates in Figure 5 seems to be continuously distributed and sharply bounded by the rheology contrasts near the PA and at the European foreland over the orogen to the west of the PL fault. Subsidence still occurs around Wolfsberg and in the Seckau area, but the subsidence close to the Fohnsdorf Basin seems to have terminated, because the

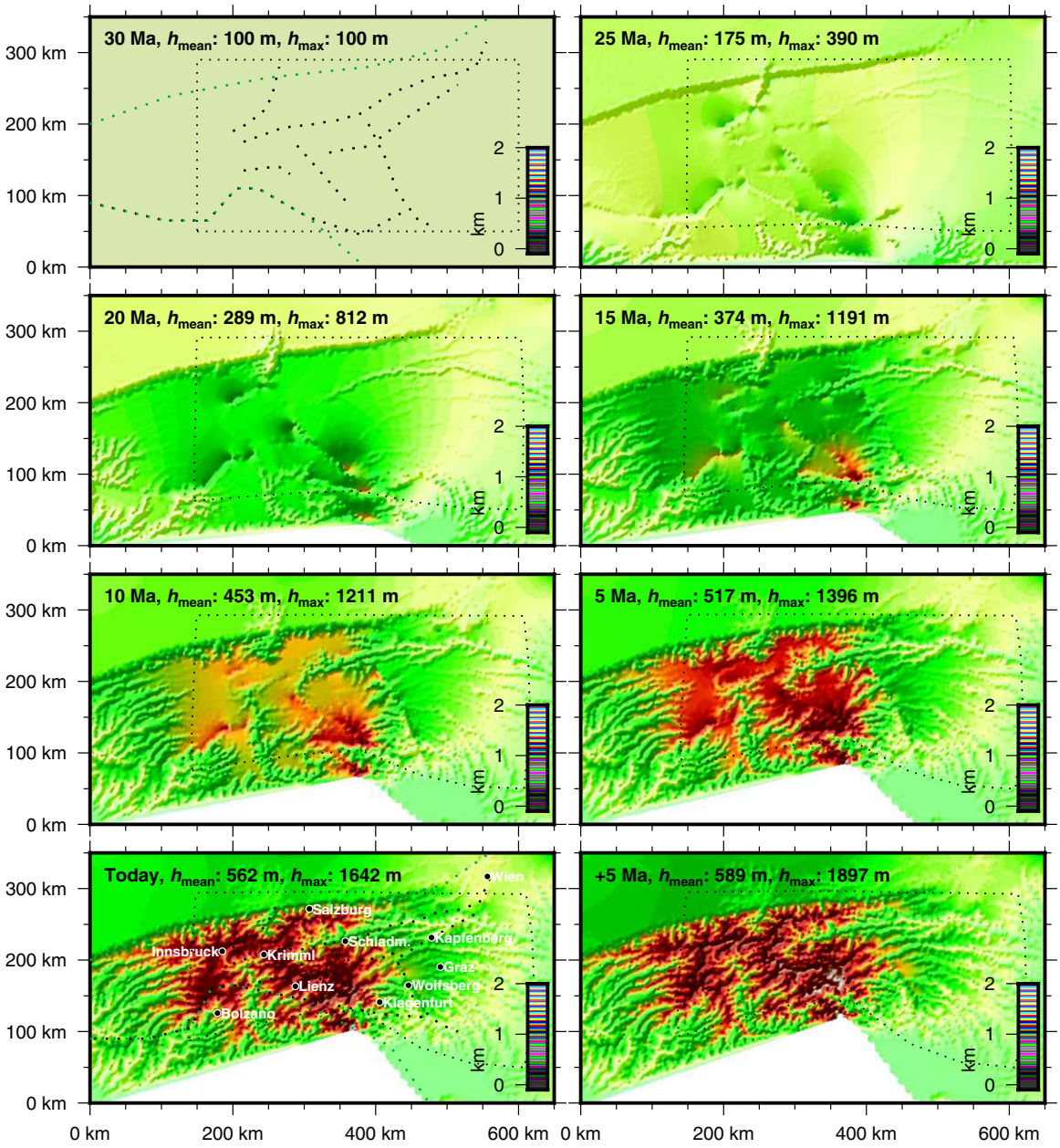

Figure 4. Simulation results of the topographic elevation development of the Eastern Alps during the past 30 m.y. until +5 m.y. The fault locations (black) and rheology contrast boundaries (green) are in dotted lines. The h_{mean} and h_{max} are the mean and maximum elevations of topography inside the dotted box, which was chosen inside the model boundaries to avoid boundary condition effects.

MM fault system is inactive and the Styrian block is further elevated in the Koralm and Gleinalm region, consistent with observations of Wölfler et al. (2011), Reischenbacher and Sachsenhofer (2013), and Strauss et al. (2001). In Figure 4 the mean height climbs to 453 m, but the peak height has barely increased to 1211 m west of Klagenfurt close to the PA. In the Pliocene (5 m.y.) the tectonic setting hardly changed; still only the PL is active. A mean elevation of 517 m and a maximum height of 1396 m is reached. At the PA, erosion built up a broad valley, which largely denudes the Southalpine. During the remainder of the model evolution no more faulting is active and uplift proceeds continuously. The mean elevation continuously increases to 562 m, while the maximum height reaches 1642 m.

The future projection of topography development to +5 m.y. from present, assuming no more active faults, shows a further increase of mean height to 589 m, which is comparable to previous steps. The maximum height, which can be found at the PA west of Klagenfurt, increases to 1897 m. This happens without any strike-slip activity.

DISCUSSION

The results of the forward modeling approach to predict the topographical evolution of the Eastern Alps show that the Miocene strike-slip faulting is profoundly and intimately related to

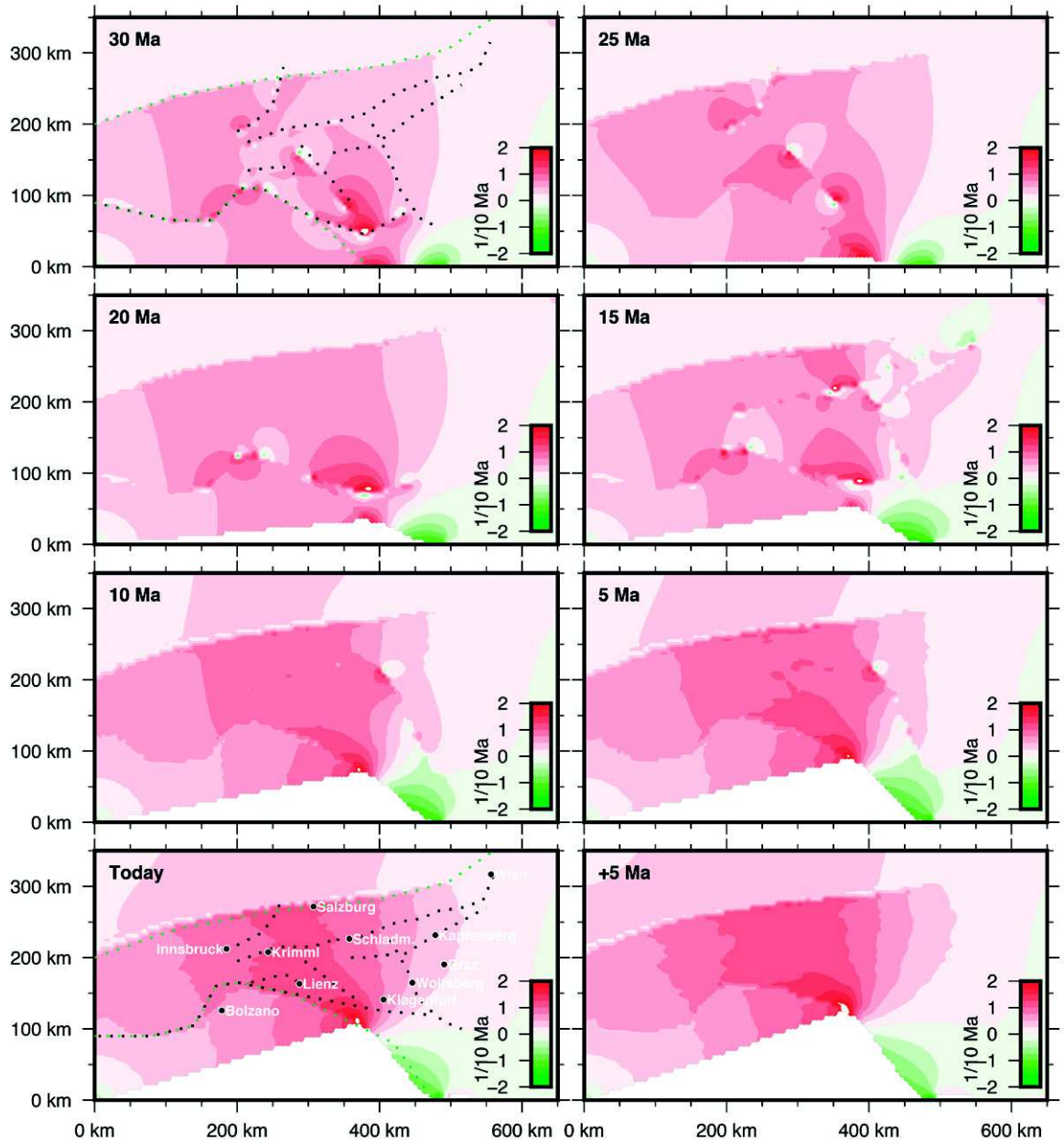

Figure 5. Vertical strain rate at the same time steps as in Figure 4. Vertical strain rate is used as a proxy for compression (red) and extension (green).

topographic uplift and drainage geometry. Most changes in mean height or the dissection of the model mountain range into individual massifs occur during the time steps at which faults are most active. In order to illustrate this further, Figure 6 shows a comparison of the topographic evolution of the model after 30 m.y. of deformation (i.e., today) between three different assumptions about the activity of faulting. Figure 6A shows the result of a model evolution without any active faults; in Figure 6B, all seven faults zones discussed are active during the entire evolution of the model run, and Figure 6C corresponds to the bottom left panel in Figure 4 (i.e., for temporally variable faulting, as discussed here). Similar to the results shown in Ratschbacher et al. (1991a, 1991b) and Robl et al. (2008b), we observe that the activity of strike-slip faulting has a strong influence on the development of topographic elevations. In general, the increase of strike-slip faulting activity (in terms of number of faults and activity duration) decreases the rate of elevation gain in the orogen. Strike-slip faulting appears to be a major process for vertical strain accumulation and increased erosion, which is responsible for the development of topographic features like valleys and mountains. The simulation without any faults (Fig. 6A) hardly reflects any features of the Eastern Alps except the buildup of a drainage, which correlates with the valley systems north of Bolzano. However, the open faulting run (Fig. 6B) resolves features like several of the Miocene intramontane basins or the Glockner massif, but hardly reproduces the uplift of the Tauern Window, especially its western end. In contrast, the temporal faulting run (Fig. 6C) exhibits most intramontane basins and the uplift of the Tauern Window reasonably well.

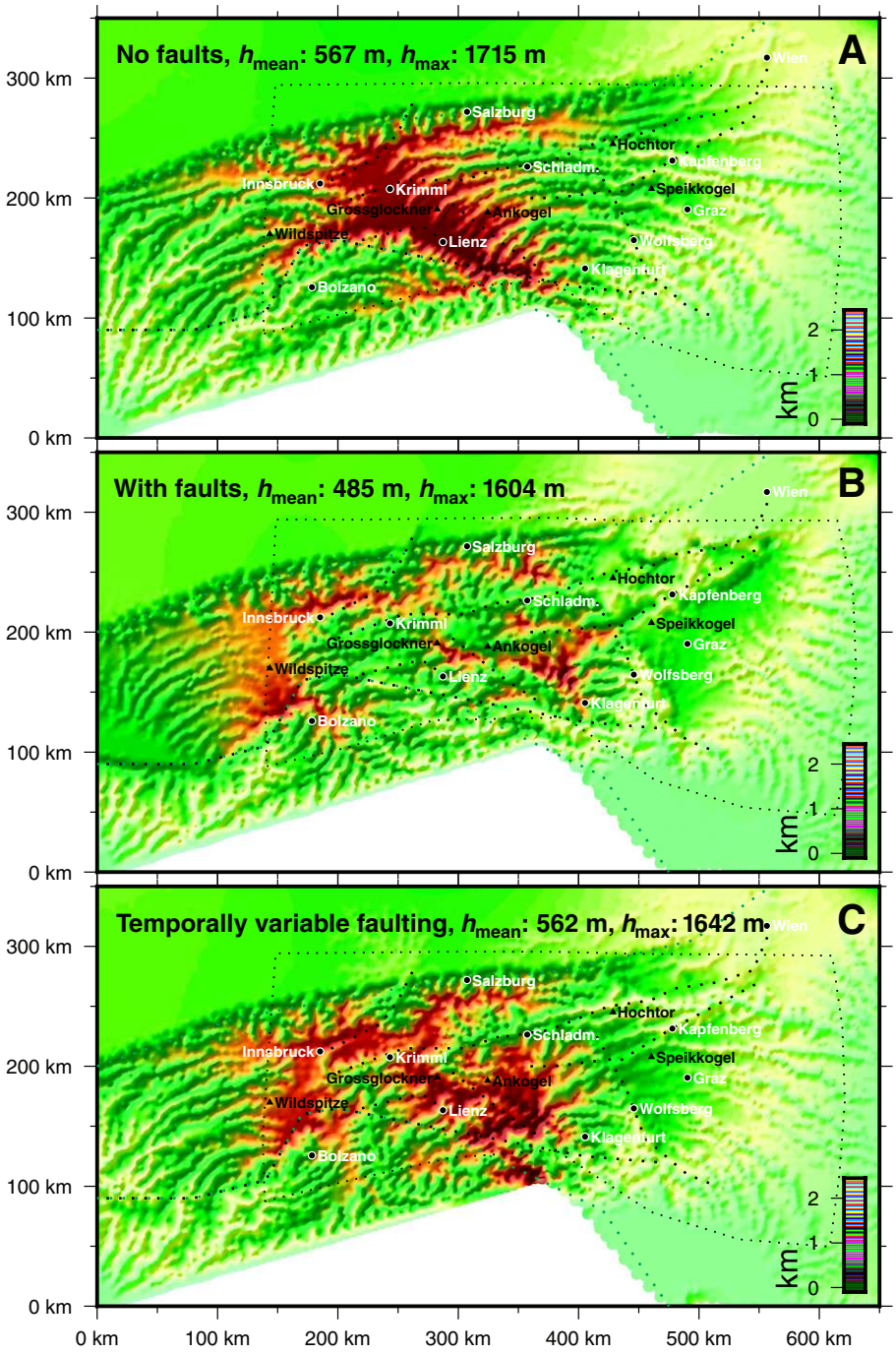

Figure 6. Comparison of the final stage of the model simulation (for today) for three different end members of faulting activity during the past 30 m.y. The h_{mean} and h_{max} are the mean and maximum elevations of topography inside the dotted box. (A) No faulting during the entire simulation for 30 m.y. (B) All seven faults considered in this study are active (open) for the entire simulation. (C) Temporally variable fault activity as shown in Figure 2, bottom left panel.

Comparison with the Topography of the Eastern Alps

Figure 7 shows that many of the primary morphological features of the Eastern Alps are reproduced by the model after 30 m.y. of evolution. This is particularly exciting as we reemphasize that the model assumes extremely simplistic boundary conditions and starts with a flat topography so that all valleys and ranges are dynamically formed by the model. However, there are also some major discrepancies. The most important primary differences between model and observed topography include the absence of topography west of Innsbruck and the unusual high topography in the region between Klagenfurt and Lienz (Fig. 7). Both shortcomings are easily explained: the lack of topography in the western part of the model region (Fig. 7) is a consequence of our boundary conditions, which do not consider convergence there. Because uplift is exclusively driven by convergence, erosion according to Equation 5 causes substantial incision of drainages toward the west, where base level remains at low elevations. Therefore, the modeled topography should not be compared in the transparently shaded region in Figure 7. Correspondingly, the modeled high plateau region between Lienz and Klagenfurt (Fig. 7B) is the consequence of maximum convergence in this model region. The absence of such topography in the Eastern Alps is interpreted to be caused by substantial glacial erosion in the Klagenfurt region (well known in this region), and by soft lithologies such as the Gurktal nape system in the region. Remnants of highly elevated plateau-like paleolandscapes outside the glacially carved and soft lithologies are found in the region (e.g., Nockberge), similar to those featured in the model.

Despite these two major discrepancies between model and nature, there are also many aspects of the topography of the Eastern Alps that are well reflected by the model. In the south a drainage system has formed in the model that resembles the Adige drainage, and a series of west-east–striking valley form in the region of the PA. In the north, west-east–running drainages akin to the Salzach, Enns, and Inn Rivers form in the model. In the eastern model region, pull-apart basins formed along the major faults, and asymmetric mountain ranges, like the Koralpe, develop. The highest elevations are located in the central model region, where the Tauern range is located. Differences between model and mountain range can be used to infer interesting aspects of the uplift history of the range that depart from the simplistic model boundary conditions.

For example, the valley incision in the western part of the SEMP is underpredicted in the simulation. One explanation is that several splay faults of this system are not considered in our model. Furthermore, the decision to model the SEMP as two separated parts probably inhibits a potential valley incision. Correspondingly, the Inn valley also appears underdeveloped in the simulation. This raises the question if the Engadine fault also needs to be regarded as a prolongation of the IN, or if there are times of activity that are still unknown. However, the IN fault is supposed to be part of a low-angle

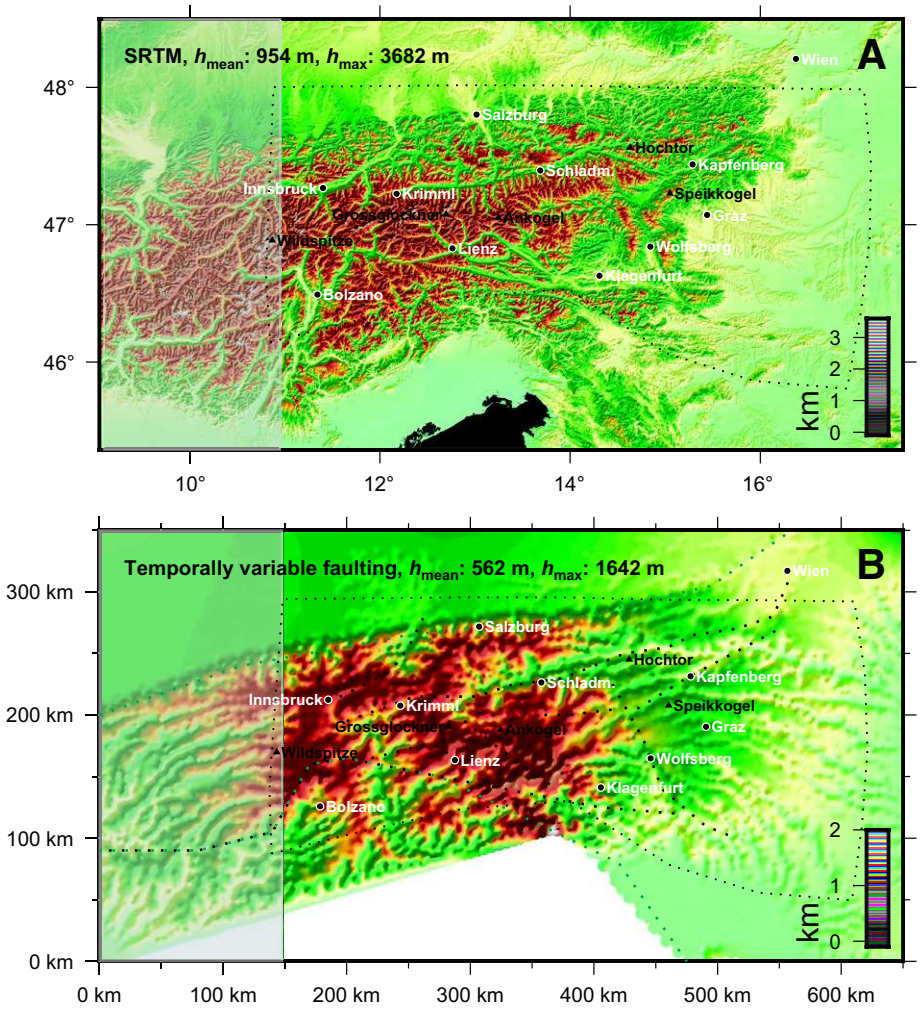

Figure 7. Topographic map of the Eastern Alps in comparison with the predicted topography of the model simulation. The h_{mean} and h_{max} are the mean and maximum elevations of topography inside the dotted box. (A) Plotted from the STRM (Shuttle Radar Topography Mission) digital elevation model (CGIAR-CSI Consultative Group on International Agricultural Research–Consortium for Spatial Information) (2014; http://srtm.csi.cgiar.org/), 250 m. (B) The modeled topography for temporally variable faults, as in Figure 4.

detachment fault (Pfiffner, 2010) and therefore does not fit the modeling constraints in Barr and Houseman (1996). Other shortcomings can also be explained by regional differences between model and local geology. Nevertheless, despite several shortcomings of the simplistic fault geometry, the model presents a major improvement over earlier models in Robl et al. (2008b).

An interesting aspect of the model results is that both the mean elevation and the maximum peak height are underpredicted by several hundreds of meters. In order to test if this is due to an overestimation of the assumed erosion rate, we reduced the erosion parameter, e, from 2500 to 1500 $m^{-1}s^{-1}$ for the temporally variable faulting run and compared it with the results shown here. Only a small elevation gain is achieved by this change, indicating that the erosion parameter in the model results shown is not the reason for this underprediction. We interpret the underprediction of mean topography by almost 400 m (Fig. 7) to be the consequence of a large-wavelength, deep-seated uplift event that is unrelated to convergence and therefore independent of our model boundary conditions. It is interesting that a similar amount of uplift was suggested from field evidence by Legrain et al. (2014), Wagner et al. (2010), and others to have occurred during a renewed uplift event of the Eastern Alps in the past 4 m.y. Atmospheric upwelling (Lippitsch et al., 2003), glacial erosion (Sternai et al., 2012), elastic rebound (Baran et al., 2014), and climate factors (Willett, 2010) are under discussion for an explanation of this event.

Evolution of Orogenic Heights and the Tauern Window

To give further insight to the topographical evolution of the orogen, the mean and maximum elevations of the simulation area for the three runs in Figure 6 are shown in Figures 8A and 8B. The mean elevation shows a stable, more or less linear growth over time for the closed and the temporally varying fault activity runs, consistent with interpretations of thermochronology. However, the open faulting run shows a slight exponential decrease of growth and an ~5% reduced final mean height. This can be interpreted as the orogen still not being in equilibrium with the erosion process, and has strong potential for further topographical growth, which is consistent with the interpretations of Hergarten et al. (2010) and Robl et al. (2015) (see the animations in Data Repository Figs. S1–S5[1]). The slight departure from linear topography growth for the variable faulting run at 15 m.y. corresponds to the time of maximum faulting activity. Thus, Figure 8A confirms the correlation of strike-slip activity with the decreasing mean elevation of the orogen. The relationship between elevation and time is different for the maximum peak heights (Fig. 8B), which are mostly observed around the southern end of the MV fault and around the PA west of Klagenfurt. Strike-slip faulting results in a substantial increase of maximum heights, compared to an orogeny without faulting (Fig. 8B) until ca. 15 m.y. Then maximum peak height stagnates completely due to erosion, while the mean elevation (large-scale uplift) is still continuously growing. Therefore, the relief (i.e., the difference between maximum and mean elevation) is predicted to be largest in the middle Miocene, which may be supported by the peak

[1]GSA Data Repository Item 2017083, Figure S1: Evolution of topography and drainage network in a zone of continental collision computed for model boundary conditions akin to the Eastern European Alps as described herein. The model is somewhat simplified from the figures in the article and consider only four major faults. Formation of topography over time. Note that faults and the rheology contrast between major tectonic units cause a spatially complex uplift pattern. Figure S2: Development of the drainage system color coded for steepness index ksn. Note the response time between topography formation and fluvial incision in the center of the orogen. Figure S3: Perspective view showing topography formation by plate convergence and crustal thickening, topography destruction by fluvial incision and lateral extrusion confined by orogen-scale strike-slip faults. Figure S4: Perspective view showing erosion rates on an evolving orogen in a zone of plate convergence. Figure S5: Perspective view showing the computational mesh color coded for erosion rates during the evolution of a mountain range driven by indenter tectonics. Available at http://www.geosociety.org/datarepository/2017, or on request from editing@geosociety.org.

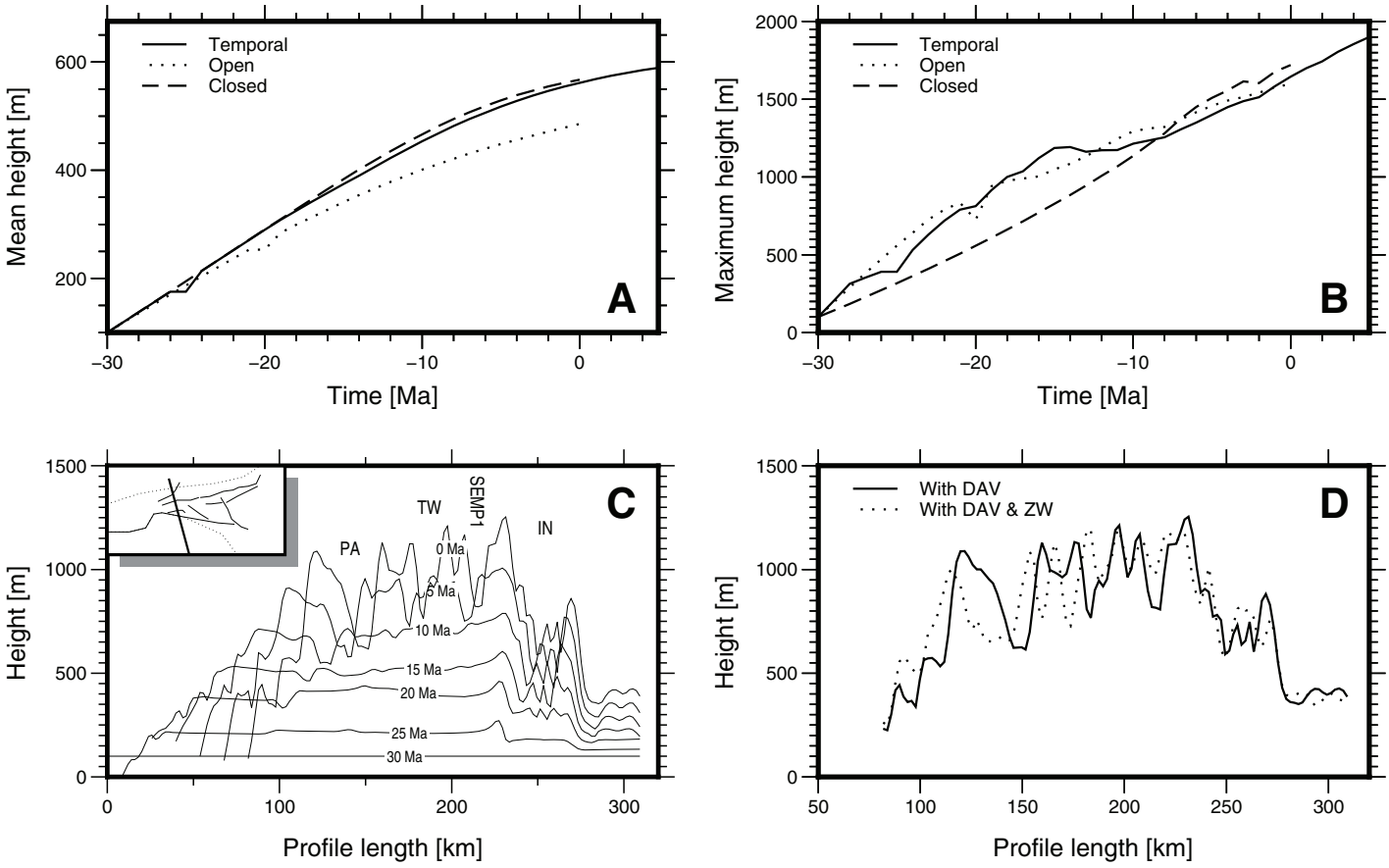

Figure 8. Predicted evolution of mean and maximum topography in the Eastern Alps and the Tauern Window profile. See Figure 2 for fault abbreviations. (A) Evolution of mean elevations of the topography measured within the 100 m contour in comparison for the simulation with open, closed, and temporally varying strike-slip faulting activity. (B) Maximum elevation of the orogen for the same three simulations. Note that maximum elevation stagnates during the peak period of lateral extrusion. (C) Profile through the Tauern Window (black line in inset), showing an over-broadened valley system along the Periadriatic fault (PA) and underpredicted valley incision along the Salzach-Ennstal-Mariazell-Puchberg fault (SEMP). The Tauern Window starts to exhume ~20 m.y. ago. (D) Two more scenarios for the topographic evolution of this profile with the Defreggen-Antholz-Vals fault (DAV) excluded and Zwischenberg-Wöllatratten fault (ZW) included. An increase of faulting at the southern end of the Tauern Window drastically broadens the Tauern range (TA).

in the sedimentation rates observed for that time (Kuhlemann et al., 2002). During the last 12 m.y. of the model evolution, the maximum elevations begin to rise again and this process is predicted to continue for the next few million years unless faulting activity commences again (cf. with the +5 m.y. snapshot in Fig. 4).

We conclude this study by investigating the model predictions for the topographic evolution of the Tauern Window region in more detail, because this region has the highest peaks, exhumes the deepest crustal level rocks of the Eastern Alps (Fig. 8C, 8D), and its exhumation history is not only subject to an active discussion about, e.g., subduction polarity changes and deep-crust collision structures (Kissling et al., 2006; Lippitsch et al., 2003), but also has implications for the formation of metamorphic domes in general. Figure 8C shows the time history of the topography along a northwest-southeast profile across the window, as shown in the inset for the model run with temporally variable fault activity (cf. Figs. 1 and 8C). The profile location crosses the model location where Figure 5 shows that crustal extension occurs at 15 m.y., consistent with the exhumation of the window at this time. It is seen that the major topographic features of the Eastern Alps are reproduced by the model. High elevations occur inside the Tauern Window, and valleys have incised along the bounding fault lines. The southern Alps (the region south of PA) are somewhat lower, while the NCA north of the IN fault are characterized by high relief. The largest differences between the model and Eastern Alps are the underprediction of elevation (as discussed here) and the much too prominent incision of the valleys around the PA. We interpret this prominent valley incision around PA to be the consequence of our simplified assumption of the fault geometry south of the Tauern Window. In the Eastern Alps, this region is characterized by a large number of small fault zones (Wölfler et al., 2012). In order to test this hypothesis, we added an additional fault zone (Zwischenberg-Wöllatratten fault) into the model in this region and explored model evolutions with this and the nearby DAV faults active versus them being inactive (Fig. 8D). The results in Figure 8D show that the overall height of the Tauern Window varies only slightly, which indicates that internal splay faults of the Tauern Window might be the controlling factor. However, the extent of the Tauern range depends on the DAV and Zwischenberg-Wöllatratten faulting. The most extended and elevated Tauern range is gained when DAV and Zwischenberg-Wöllatratten fault are introduced into the model.

In summary, it may be said that the exhumation of the Tauern Window and the elevation

of the Tauern range are largely controlled by the activity of the Miocene fault lines that bound the region to the north and south. The low-angle detachments that bound the Tauern Window to the west and east (Brenner normal fault; Fügenschuh et al., 1997, and Katschberg normal fault; Genser and Neubauer, 1989) form passively only on its eastern end in response to the fault activity (see also Fig. 5 at 15 m.y.) and need not be considered explicitly in the model. This interpretation has implications for the exhumation of metamorphic core complexes in general. Originally, core complexes were only thought to be exhumed in extensional environments (Lister and Davis, 1989). Later studies showed that core complexes are also exhumed in transpressional (Fritz et al., 2002) or strike-slip environments (Meyer et al., 2014). The current mechanical considerations show that low-angle detachments exhuming metamorphic domes may form passively in response to slip zones bounding the domes, and therefore widen the number of tectonic regimes in which core complexes may form.

CONCLUSIONS

Our modeling study confirms the strong influence of temporally variable Miocene strike-slip fault activity on the topography of the Eastern Alps. It is shown that strike-slip activity moderately slows the mean surface uplift of the orogen in the Miocene, but emphasizes the rise of peak elevations during the peak time of faulting, ca. 15 m.y. Therefore, Miocene faulting is one major driver for the buildup of reliefs in the topographic evolution of the Eastern Alps.

Time-series analysis of the model evolution of topography shows that many of the primary features of today's topography are reproduced by the model, including the major west-east–striking valleys in the north of the range, the plateau-like topography at high elevations (see animations in Figs. S1–S5), the south-draining valley systems near Bolzano, and the intramontane basins at the eastern end of the Alps. Conversely, several shortcomings of the model can be accommodated by more refined model assumptions of fault geometry. Many of the model assumption, for example, that there was no significant relief or topography ca. 30 m.y., appear to be justified.

Our model underpredicts the mean topography of the Alps by several hundreds of meters and predicts a lack of geomorphic equilibrium in the range. This is supported by field studies of Wagner et al. (2011), Legrain et al. (2014), and others who inferred a rejuvenation of the uplift in the past 5 m.y., and is interpreted due to a post–5 m.y., large-wavelength, deep-seated surface uplift event that currently affects the eastern end of the Alps independent of convergence. It is also consistent with the inference of Hergarten et al. (2010) that the Eastern Alps are morphologically immature and still growing.

Exhumation of the Tauern Window and the associated uplift of the Tauern range in the center of the Eastern Alps are strongly linked to west-east–striking slip faults to the north and south. The low-angle detachments bounding the window to the west and east (Brenner and Katschberg faults) develop passively in response to the strike-slip faulting. Our model predicts that metamorphic domes need not form exclusively in extensional settings, but may be related to transpressional or strike-slip regimes.

ACKNOWLEDGMENTS

We thank L. Evans, Monash University, for her support in implementing advancements in the fault functionality into the finite element code used here; H. Fritz, University of Graz, for discussions about faulting history in the Eastern Alps; and G. Houseman, University of Leeds, for his explanations of the thin sheet formulation. We also thank two anonymous reviewers, and A. Weil for editorial handling.

REFERENCES CITED

Baran, R., Friedrich, A.M., and Schlunegger, F., 2014, The late Miocene to Holocene erosion pattern of the Alpine foreland basin reflects Eurasian slab unloading beneath the western Alps rather than global climate change: Lithosphere, v. 6, p. 124–131, doi:10.1130/L307.1.

Barr, T.D., and Houseman, G., 1996, Deformation fields around a fault embedded in a non-linear ductile medium: Geophysical Journal International, v. 125, p. 473–490, doi:10.1111/j.1365-246X.1996.tb00012.x.

Brückl, E., Behm, M., Decker, K., Grad, M., Guterch, A., Keller, G., and Thybo, H., 2010, Crustal structure and active tectonics in the Eastern Alps: Tectonics, v. 29, TC2011, doi:10.1029/2009TC002491.

Champagnac, J., Molnar, P., Anderson, R., Sue, C., and Delacou, B., 2007, Quaternary erosion-induced isostatic rebound in the western Alps: Geology, v. 35, p. 195–198, doi:10.1130/G23053A.1.

Decker, K., Peresson, H., and Faupl, P., 1994, Die miozäne Tektonik der östlichen Kalkalpen: Kinematik, Paläospannungen und Deformationsaufteilung während der "lateralen Extrusion" der Zentralalpen: Jahrbuch der Geologischen Bundesanstalt, v. 137, p. 5–18.

Dunkl, I., Kuhlemann, J., Reinecker, J., and Frisch, W., 2005, Cenozoic relief evolution of the Eastern Alps—Constraints from apatite fission track age-provenance of Neogene intramontane sediments: Australian Journal of Earth Sciences, v. 98, p. 92–105.

England, P., and Houseman, G., 1986, Finite strain calculations of continental deformation 2. Comparison with the India-Asia collision zone: Journal of Geophysical Research, v. 91, p. 3664–3676, doi:10.1029/JB091iB03p03664.

England, P., and McKenzie, D., 1982, A thin viscous sheet model for continental deformation: Royal Astronomical Society Geophysical Journal, v. 70, p. 295–321, doi:10.1111/j.1365-246X.1982.tb04969.x.

England, P., and McKenzie, D., 1983, A thin viscous sheet model for continental deformation: Correction: Royal Astronomical Society Geophysical Journal, v. 73, p. 523–532, doi:10.1111/j.1365-246X.1983.tb03328.x.

Frisch, W., Kuhlemann, J., Dunkl, I., and Brügel, A., 1998, Palinspastic reconstruction and topographic evolution of the Eastern Alps during late Tertiary tectonic extrusion: Tectonophysics, v. 297, p. 1–15, doi:10.1016/S0040-1951(98)00160-7.

Frisch, W., Dunkl, I., and Kuhlemann, J., 2000, Post-collisional orogen-parallel large scale extension in the Eastern Alps: Tectonophysics, v. 327, p. 239–265, doi:10.1016/S0040-1951(00)00204-3.

Fritz, H., Dallmeyer, D.R., Wallbrecher, E., Loizenbauer, J., Hoinkes, G., Neumayr, P., and Khudir, A.A., 2002, Neoproterozoic tectonothermal evolution of the central Eastern Desert, Egypt: A slow velocity tectonic process of core complex exhumation: Journal of African Earth Sciences, v. 34, p. 137–155, doi:10.1016/S0899-5362(02)00014-3.

Froitzheim, N., Plasienka, D., and Schuster, R., 2008, Alpine tectonics of the Alps and Western Carpathians, *in* McCann, T., ed., The geology of Central Europe, Volume 2: Mesozoic and Cenozoic: London, Geological Society, p. 1141–1232.

Frost, E., Dolan, J., Sammis, C., Hacker, B., Cole, J., and Ratschbacher, L., 2009, Progressive strain localization in a major strike-slip fault exhumed from midseismogenic depths: Structural observations from the Salzach-Ennstal-Mariazell-Puchberg fault system, Austria: Journal of Geophysical Research, v. 114, B04406, doi:10.1029/2008JB005763.

Fügenschuh, B., Seward, D., and Mancktelow, N., 1997, Exhumation in a convergent orogen: The western Tauern window: Terra Nova, v. 9, p. 213–217, doi:10.1046/j.1365-3121.1997.d01-33.x.

Genser, J., and Neubauer, F., 1989, Low angle normal faults at the eastern margin of the Tauern window (Eastern Alps): Mitteilung der Österreichischen Geologischen Gesellschaft, v. 81, p. 233–243.

Genser, J., Cloetingh, S.A., and Neubauer, F., 2007, Late orogenic rebound and oblique Alpine convergence: New constraints from subsidence analysis of the Austrian Molasse basin: Global and Planetary Change, v. 58, p. 214–223, doi:10.1016/j.gloplacha.2007.03.010.

Glodny, J., Ring, U., and Kühn, A., 2008, Coeval high-pressure metamorphism, thrusting, strike-slip, and extensional shearing in the Tauern Window, Eastern Alps: Tectonics, v. 27, TC4004, doi:10.1029/2007TC002193.

Handy, M.R., Schmid, S.M., Bousquet, R., Kissling, E., and Bernoulli, D., 2010, Reconciling plate-tectonic reconstructions of Alpine Tethys with the geological-geophysical record of spreading and subduction in the Alps: Earth-Science Reviews, v. 102, p. 121–158, doi:10.1016/j.earscirev.2010.06.002.

Hergarten, S., Wagner, T., and Stüwe, K., 2010, Age and prematurity of the Alps derived from topography: Earth and Planetary Science Letters, v. 297, p. 453–460, doi:10.1016/j.epsl.2010.06.048.

Horvath, F., and Cloetingh, S., 1996, Stress-induced late-stage subsidence anomalies in the Pannonian basin: Tectonophysics, v. 266, p. 287–300, doi:10.1016/S0040-1951(96)00194-1.

Houseman, G., and England, P., 1986, Finite strain calculation of continental deformation: 1. Method and general results for convergent zones: Journal of Geophysical Research, v. 91, p. 3651–3663, doi:10.1029/JB091iB03p03651.

Inger, S., and Cliff, A., 1994, Timing of metamorphism in the Tauern Window, Eastern Alps: Rb-Sr ages and fabric formation: Journal of Metamorphic Geology, v. 12, p. 695–707, doi:10.1111/j.1525-1314.1994.tb00052.x.

Kissling, E., Schmid, S.M., Lippitsch, R., Ansorge, J., and Fügenschuh, B., 2006, Lithosphere structure and tectonic evolution of the Alpine arc: New evidence from high-resolution teleseismic tomography, *in* Gee, D.G., and Stephenson, R.A., eds., European lithosphere dynamics: Geological Society, London, Memoir 32, p. 129–145, doi:10.1144/GSL.MEM.2006.032.01.08.

Kuhlemann, J., 2007, Paleogeographic and paleotopographic evolution of the Swiss and Eastern Alps since the Oligocene: Global and Planetary Change, v. 58, p. 224–236, doi:10.1016/j.gloplacha.2007.03.007.

Kuhlemann, J., Frisch, W., Dunkl, I., and Székely, B., 2001, Quantifying tectonic versus erosive denudation by the sediment budget: The Miocene core complexes of the Alps: Tectonophysics, v. 330, p. 1–23, doi:10.1016/S0040-1951(00)00209-2.

Kuhlemann, J., Frisch, W., Székely, B., and Dunkl, I., 2002, Post-collisional sediment budget history of the Alps: Tectonic versus climatic control: International Journal of Earth Sciences, v. 91, p. 818–837, doi:10.1007/s00531-002-0266-y.

Kurz, W., Wölfler, A., Rabitsch, R., and Genser, J., 2011, Polyphase movement on the Lavanttal fault zone (Eastern Alps): Reconciling the evidence from different geochronological indicators: Swiss Journal of Geoscience, v. 104, p. 323–343, doi:10.1007/s00015-011-0068-y.

Legrain, N., Stüwe, K., and Wölfer, A., 2014, Incised relict landscapes in the eastern Alps: Geomorphology, v. 221, p. 124–138, doi:10.1016/j.geomorph.2014.06.010.

Linzer, H.G., Decker, K., Peresson, H., Dell'Mour, R., and Frisch, W., 2002, Balancing lateral orogenic float of the Eastern Alps: Tectonophysics, v. 354, p. 211–237, doi:10.1016/S0040-1951(02)00337-2.

Lippitsch, R., Kissling, E., and Ansorge, J., 2003, Upper mantle structure beneath the Alpine orogen from high-resolution teleseismic tomography: Journal of Geophysical Research, v. 108, 2376, doi:10.1029/2002JB002016.

Lister, G.S., and Davis, G.A., 1989, The origin of metamorphic core complexes and detachment faults formed during Tertiary continental extension in the northern Colorado River region, U.S.A?: Journal of Structural Geology, v. 11, p. 65–94, doi:10.1016/0191-8141(89)90036-9.

Mancktelow, N.S., Stöckli, D.F., Grollimund, B., Müller, W., Fügenschuh, B., Viola, G., Seward, D., and Villa, I.M., 2001, The DAV and Periadriatic fault systems in the Eastern Alps south of the Tauern window: International Journal of Earth Sciences, v. 90, p. 593–622, doi:10.1007/s005310000190.

Meyer, S.E., Passchier, C., Abu-Alam, T., and Stüwe, K., 2014, A strike-slip core complex from the Najd fault system, Arabian shield: Terra Nova, v. 26, p. 387–394, doi:10.1111/ter.12111.

Müller, W., Mancktelow, N.S., and Meier, M., 2000, Rb-Sr microchrons of synkinematic mica in mylonites: An example from the DAV fault of the Eastern Alps: Earth and Planetary Science Letters, v. 180, p. 385–397, doi:10.1016/S0012-821X(00)00167-9.

Müller, W., Prosser, G., Mancktelow, N.S., Villa, I.M., Kelly, S.P., Viola, G., and Oberli, F., 2001, Geochronological constraints on the evolution of the Periadriatic fault system (Alps): International Journal of Earth Sciences, v. 90, p. 623–653, doi:10.1007/s005310000187.

Nocquet, J.M., and Calais, E., 2003, Crustal velocity field of western Europe from permanent GPS array solutions, 1996–2001: Geophysical Journal International, v. 154, p. 72–88, doi:10.1046/j.1365-246X.2003.01935.x.

Pfiffner, O.A., 2010, Geologie der Alpen: Bern, Haupt Verlag, 360 p.

Plan, L., Grasemann, B., Spötl, C., Decker, K., Boch, R., and Kramers, J., 2010, Neotectonic extrusion of the Eastern Alps: Constraints from U/Th dating of tectonically damaged speleothems: Geology, v. 38, p. 483–486, doi:10.1130/G30854.1.

Pleuger, J., Mancktelow, N., Zwingmann, H., and Manser, M., 2012, K-Ar dating of synkinematic clay gouges from Neoalpine faults of the Central, Western and Eastern Alps: Tectonophysics, v. 550–553, p. 1–16, doi:10.1016/j.tecto.2012.05.001.

Ratschbacher, L., Merle, O., Davy, P., and Cobbold, P., 1991a, Lateral extrusion in the Eastern Alps, part 1: Boundary conditions and experiments scaled for gravity: Tectonics, v. 10, p. 245–256, doi:10.1029/90TC02622.

Ratschbacher, L., Frisch, W., and Linzer, H.G., 1991b, Lateral extrusion in the Eastern Alps, part 2: Structural analysis: Tectonics, v. 10, p. 257–271, doi:10.1029/90TC02623.

Reinecker, J., 2000, Stress and deformation: Miocene to present-day tectonics in the Eastern Alps: Tübinger Geowissenschafliche Arbeiten Volume 55, Reihe A: Institut und Museum für Geologie und Paläontologie der Universität Tübingen, 156 p.

Reischenbacher, D., and Sachsenhofer, R.F., 2013, Basin formation during the post collisional evolution of the Eastern Alps: The example of the Lavanttal Basin: International Journal of Earth Sciences, v. 102, p. 517–543, doi:10.1007/s00531-012-0807-y.

Reischenbacher, D., Rifelj, H., Sachsenhofer, R.F., Jelen, B., Coric, S., Gross, M., and Reichenbacher, B., 2007, Early Badenian paleoenvironment in the Lavanttal Basin (Mühldorf Formation; Austria): Evidence from geochemistry and paleontology: Australian Journal of Earth Sciences, v. 100, p. 202–229.

Robl, J., and Stüwe, K., 2005a, Continental collision with finite indenter strength: 1. Concept and model formulation: Tectonics, v. 24, TC4005, doi:10.1029/2004TC001727.

Robl, J., and Stüwe, K., 2005b, Continental collision with finite indenter strength: 2. European Eastern Alps: Tectonics, v. 24, TC4014, doi:10.1029/2004TC001741.

Robl, J., Hergarten, S., and Stüwe, K., 2008a, Morphological analysis of the drainage system in the Eastern Alps: Tectonophysics, v. 460, p. 263–277, doi:10.1016/j.tecto.2008.08.024.

Robl, J., Stüwe, K., Hergarten, S., and Evans, L., 2008b, Extension during continental convergence in the Eastern Alps: The influence of orogen-scale strike-slip faults: Geology, v. 36, p. 963–966, doi:10.1130/G25294A.1.

Robl, J., Prasicek, G., Hergarten, S., and Stüwe, K., 2015, Alpine topography in the light of tectonic uplift and glaciation: Global and Planetary Change, v. 127, p. 34–49, doi:10.1016/j.gloplacha.2015.01.008.

Rosenberg, C.L., and Schneider, S., 2008, The western termination of the SEMP fault (eastern Alps) and its bearing on the exhumation of the Tauern Window, *in* Siegesmund, S., et al., eds., Tectonic aspects of the Alpine-Dinaride-Carpathian System: Geological Society, London, Special Publication 298, p. 197–218, doi:10.1144/SP298.10.

Royden, L., Horvath, F., and Rumpler, J., 1983, Evolution of the Pannonian Basin System: 2. Subsidence and thermal history: Tectonics, v. 2, p. 91–137, doi:10.1029/TC002i001p00091.

Sachsenhofer, R.F., Bechtel, A., Reischenbacher, D., and Weiss, A., 2003, Evolution of lacustrine systems along the Miocene Mur-Mürz fault system (Eastern Alps, Austria) and implications on source rocks in pull-apart basins: Marine and Petroleum Geology, v. 20, p. 83–110, doi:10.1016/S0264-8172(03)00018-7.

Schneider, S., Hammerschmidt, K., and Rosenberg, C., 2007, In-situ Rb-Sr dating of the SEMP mylonites, western Tauern Window, Eastern Alps: Geophysical Research Abstracts, v. 9, 09136, doi:10.13140/2.1.3160.3202.

Sternai, P., Herman, F., Champagnac, J.D., Fox, M., Salcher, B., and Willett, S.D., 2012, Pre-glacial topography of the European Alps: Geology, v. 40, p. 1067–1070, doi:10.1130/G33540.1.

Strauss, P., Wagreich, M., Decker, K., and Sachsenhofer, R.F., 2001, Tectonics and sedimentation in the Fohnsdorf-Seckau Basin (Miocene, Austria): From a pull-apart basin to a half-graben: International Journal of Earth Sciences, v. 90, p. 549–559, doi:10.1007/s005310000180.

Stüwe, K., 2007, Geodynamics of the lithosphere (second edition): Berlin, Springer-Verlag, 493 p.

Stüwe, K., Robl, J., Hergarten, S., and Evans, L., 2008, Modeling the influence of horizontal advection, deformation, and late uplift on the drainage development in the India-Asia collision zone: Tectonics, v. 27, TC6011, doi:10.1029/2007TC002186.

Urbanek, C., Frank, W., Grasemann, B., and Decker, K., 2002, Eoalpine versus Tertiary deformation: Dating of heterogeneously partitioned strain (Tauern Window, Austria) [poster]: Salzburg, Pangeo 2002, http://web400.login-3.hoststar.at/www.christoph_urbanek.at/images/POSTER.PANGEO.SEMP.2002.pdf.

Wagner, T., Fabel, D., Fiebig, M., Häuselmann, P., Sahy, D., Xu, S., and Stüwe, K., 2010, Young uplift in the non-glaciated parts of the Eastern Alps: Earth and Planetary Science Letters, v. 295, p. 159–169, doi:10.1016/j.epsl.2010.03.034.

Wagner, T., Fritz, H., Stüwe, K., Nestroy, O., Rodnight, H., Hellstrom, J., and Benischke, R., 2011, Correlations of cave levels, stream terraces and planation surfaces along the River Mur—Timing of landscape evolution along the eastern margin of the Alps: Geomorphology, v. 134, p. 62–78, doi:10.1016/j.geomorph.2011.04.024.

Willett, S.D., 2010, Late Neogene erosion of the Alps: A Climate Driver?: Annual Review of Earth and Planetary Sciences, v. 38, p. 411–437, doi:10.1146/annurev-earth-040809-152543.

Wobus, C., Whipple, K., Kirby, E., Snyder, N., Johnson, J., Spyropolou, K., Crosby, B., and Sheehan, D., 2006, Tectonics from topography: Procedures, promise, and pitfalls, *in* Willett, S.D., et al., eds., Tectonics, climate, and landscape evolution: Geological Society of America Special Paper 398, p. 55–74, doi:10.1130/2006.2398(04).

Wölfler, A., Kurz, W., Fritz, H., and Stüwe, K., 2011, Lateral extrusion in the Eastern Alps revisited: Refining the model by thermochronological, sedimentary, and seismic data: Tectonics, v. 30, TC4006, doi:10.1029/2010TC002782.

Wölfler, A., Stüwe, K., Danisik, M., and Evans, N.J., 2012, Low temperature thermochronology in the Eastern Alps: Implications for structural and topographic evolution: Tectonophysics, v. 541–543, p. 1–18, doi:10.1016/j.tecto.2012.03.016.

Zwingmann, H., and Mancktelow, N., 2004, Timing of Alpine fault gouges: Earth and Planetary Science Letters, v. 223, p. 415–425, doi:10.1016/j.epsl.2004.04.041.

MANUSCRIPT RECEIVED 15 JULY 2016
REVISED MANUSCRIPT RECEIVED 17 NOVEMBER 2016
MANUSCRIPT ACCEPTED 7 DECEMBER 2016

Printed in the USA